Debris-Covered Glaciers (Proceedings of a workshop held at Seattle, Washington, USA, September 2000). IAHS Publ. no. 265, 2000.

Role of supraglacial ponds in the ablation process of a debris-covered glacier in the Nepal Himalayas

AKIKO SAKAI

Institute for Hydrospheric–Atmospheric Sciences, Nagoya University, Furo-cho, Chikusa-ku, Nagoya 464-8601, Japan

e-mail: shakai@ihas.nagoya-u.ac.jp

NOZOMU TAKEUCHI*

Basic Biology, Faculty of Bioscience and Biotechnology (c/o Faculty of Science), Tokyo Institute of Technology, 2-12-1, O-okayama, Meguro-ku, Tokyo 152-8551, Japan

KOJI FUJITA & MASAYOSHI NAKAWO

Institute for Hydrospheric–Atmospheric Sciences, Nagoya University, Furo-cho, Chikusa-ku, Nagoya 464-8601, Japan

Abstract There are many supraglacial ponds on debris-covered glaciers in the Nepal Himalayas. The heat absorbed at the surface of a pond was estimated from heat budget observations on the Lirung Glacier in Langtang Valley, Nepal. The results indicated an average heat absorption of 170 W m^{-2} during the summer monsoon season. This rate is about 7 times the average for the whole debris-covered zone. Analysis of the heat budget for a pond suggests that at least half of the heat absorbed at a pond surface is released with the water outflow from the pond, indicating that the water warmed in the pond enlarges the englacial conduit that drains water from the pond and produces internal ablation. Furthermore, the roof of the conduit could collapse, leading to the formation of ice cliffs and new ponds, which would accelerate the ablation of the debris-covered glacier.

INTRODUCTION

In the Himalayas almost all large valley glaciers with lengths of several kilometres are covered with debris in their ablation zone. These types of glaciers occupy more than 80% of the glacier area in the Himalayas (Fujii & Higuchi, 1977). It is necessary, therefore, to examine the ablation process of debris-covered glaciers for assessment of their changes with climate and impact on water resources.

It has long been realized that a thin debris layer on a glacier surface enhances the ablation of the ice underneath, whereas thick debris inhibits melting (e.g. Østrem, 1959; Fujii, 1977; Mattson *et al.*, 1993). Inoue & Yoshida (1980) measured the ablation rate on the debris-covered zone at a number of points across the width of the glacier. Nakawo *et al.* (1993) and Rana *et al.* (1997) established a model to estimate the average melt rate for a rather large area of a debris-covered glacier by using surface temperature data estimated from satellite imagery.

* *Now at*: Frontier Observational Research System for Global Change, International Arctic Research Center, University of Alaska at Fairbanks, 930 Koyukuk Drive, PO Box 757335, Fairbanks, Alaska, USA.

There are many ice cliffs and ponds on debris-covered glaciers. Eyles (1979) and Iwata *et al.* (1980) indicated that the ablation rate of ice cliffs around a supraglacial pond is higher than that of thick debris-covered glacier ice. The ablation rate was found to be about 10 times higher at ice cliffs than the average for the whole debris-covered zone (Sakai *et al.*, 1998). However, there have been no studies of the ablation process at supraglacial ponds, and the morphological evolution due to heterogeneous ablation remains unclear. In this paper, we examine the heat absorbed at the water surface of a supraglacial pond, the pond heat balance, and the consequent effect on ice ablation.

DESCRIPTION OF OBSERVATIONS

Observations were carried out on the Lirung Glacier in Langtang Valley, Nepal. The accumulation zone is debris free. On the other hand, the ablation zone is covered with debris. Figure 1 shows a schematic map of supraglacial ponds and ice cliffs located in the ablation zone of the glacier. There were 53 ponds. Seventeen were partly surrounded by ice cliffs of 3–20 m in height (Aoki & Asahi, 1998). Figure 2 shows a photograph of one of the supraglacial ponds with an ice cliff.

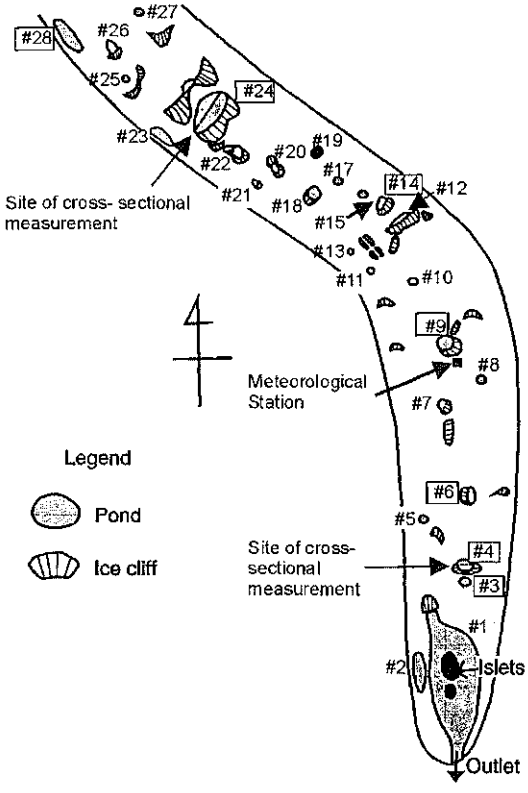

Fig. 1 Schematic map of main observed ponds and ice cliff distribution at ablation zone on the Lirung Glacier. The sign # indicates the number of the pond. Ponds where water temperature and relative water level were observed intermittently are indicated by pond numbers enclosed in a box. The cross-section and water temperature distribution were measured at pond #4 and #24.

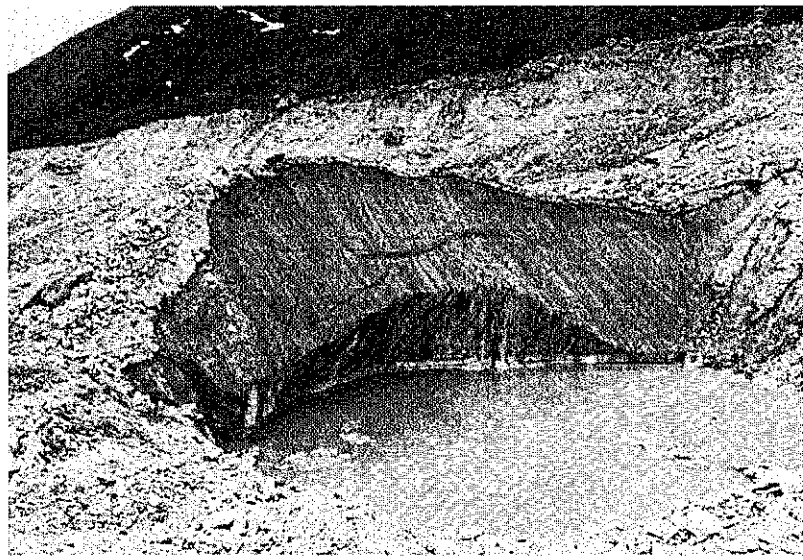

Fig. 2 Photo of one of the supraglacial ponds (#22) on the Lirung Glacier. The pond is surrounded by a debris slope and the ice cliff faces north.

Surface and bottom water temperature and water level were observed at several ponds (#3, #4, #6, #9, #14, #24 and #28) at intervals of 1 h for several days. Measurement accuracy was ±0.4°C for temperature and ±2 mm for water level. Cross-sections of two ponds with ice cliffs were measured with a tape at 1-m intervals horizontally along a line across the pond (#24 on 14 June and #4 on 13 July). A meteorological station was installed in the central part of the debris-covered zone (Fig. 1). Air temperature, relative humidity, wind speed, surface temperature of the supraglacial debris, downward and upward solar radiation, and net radiation were monitored at an interval of 5 min from 11 May to 23 October 1996, including the summer monsoon season. Respective errors were ±0.12°C, ±4%, 0.024 m s^{-1}, ±2°C, 4 W m^{-2}, 0.4 W m^{-2}, and 7 W m^{-2}. Details of observations and preliminary results were described by Fujita *et al.* (1997).

HEAT TRANSFER ON THE GLACIER SURFACE

Heat balance of supraglacial ponds

The water level in ponds varied diurnally. The ponds receive water from a surrounding surface watershed and discharge water through englacial conduits. It is necessary, therefore, to take into account the heat associated with the inflow to and outflow from the pond. The heat storage S of the pond is changed by the net heat input at the water surface Q, by advection from meltwater inflow I, by heat lost with the water outflow D, by latent heat for icemelt under the debris layer M_d, and bare ice in the pond, M_i (Fig. 3). The heat balance for the pond is given by:

$$\frac{\mathrm{d}S}{\mathrm{d}t} = Q + I - D - M_d - M_i \tag{1}$$

where t is time. The melting point of ice (0°C) is taken as the reference for heat content, and hence water at melting point is regarded here as containing no heat. The water temperature of meltwater inflow is probably 0°C, since it is supplied from the ice–debris interface or englacial water channels. Hence the heat with inflow I is zero. The heats M_d and M_i enlarge the pond and produce ablation. The discharged heat D enlarges the outflow water channels and produces internal ablation.

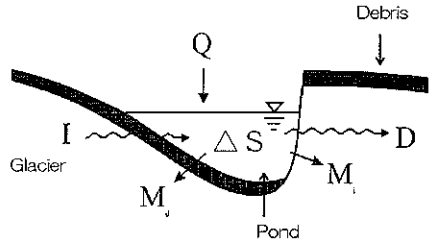

Fig. 3 Schematic figure of the heat balance at a supraglacial pond. ΔS: The change in heat storage of the pond; Q: net heat input at the water surface; D: the heat released from the outflow; I: the heat by meltwater inflow into the pond; M_d: the latent heat of fusion for icemelt under the debris layer at the bottom of the pond; and M_i: for icemelt at exposed ice cliff under the water surface.

Change of stored heat in ponds, dS/dt

Figure 4 shows the daily fluctuations in water level and water temperature (bottom and surface) for pond #6 from 28 May to 6 June. The mean bottom and surface water temperatures were similar, since the bottom ice was insulated by a thick debris layer

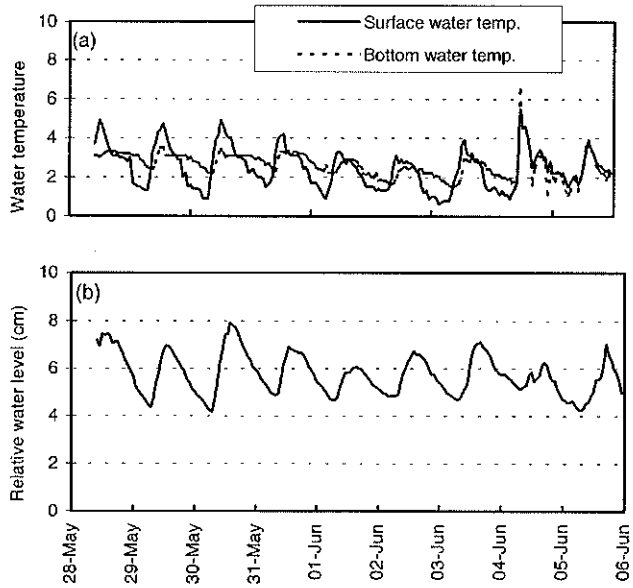

Fig. 4 Fluctuations (a) in water temperatures at the surface and bottom and (b) relative water level observed at pond #6 from 28 May to 5 June at hourly intervals.

(about 1 m). The temperature varied more at the surface than the bottom. Similar diurnal fluctuations were also observed at the other ponds.

The stored heat in the pond is given by:

$$S = c_w \rho_w T_i(t) A z_i(t) \quad (2)$$

Here c_w is the specific heat of water (= 4.2×10^3 J °C^{-1} kg^{-1}) and ρ_w is the water density (= 1000 kg m^{-3}). A and z_i represent the area and the mean depth of the pond, where A is assumed to be independent of the water level.

The average depth and the surface length were 5 m and 70 m, respectively, at a supraglacial pond near Tsho Rolpa Glacier Lake in Rolwaling Valley. These dimensions were measured at only two ponds on the Lirung Glacier, averaging about 7 m in depth and 90 m in length at pond #24, and 1.6 m and 15.5 m at pond #4, respectively. The ratio of the average depth to the surface length, β, ranged from 0.07 to 0.10. The depth of the other ponds where the water depth was not measured was estimated from the surface geometry by assuming β to be 0.08 as listed in Table 1.

The change in stored heat was calculated for each pond at 1-h intervals using equation (2) and the data for surface temperature and water level. Since the relative water level and water temperature fluctuated with relatively small amplitudes, the mean values of dS/dt averaged over a number of days were usually negligibly small with an upper limit of 4.5 W m^{-2} (Table 1).

Table 1 Size of ponds, bare ice areas, heat transfer coefficient and average calculated heat components at these ponds during each observation period. Changes in storage heat, dS/dt, less than 10^{-2} W m^{-2} were indicated by ~0. Heat with outflow, D, was calculated as the residual value of Q, M_i and M_d from equation (1).

Pond no.	Period	Pond surface area	Average pond depth	Exposed ice area	Bulk heat transfer coefficient	dS/dt	Q	M_d	M_i	D
		(m^2)	(m)	(m^2)	$\times 10^{-3}$	(W m^{-2})	(W m^{-2})	(W m^{-2})	(W m^{-2})	(W m^{-2})
#3	10–22 May	45	0.4*	0	2.06	–0.5	148	1.8	0	147
#4	10–18 May	204	1.6	31	1.79	~0	144	1.2	38	105
	17 July–5 Sept.					–2.0	192	0.9	29	164
#6	28 May–5 June	385	1.0*	15	1.86	~0	156	1.1	10	145
#9	28 May–3 June	113	1.1*	15	1.86	~0	171	1.4	41	129
#14	2–6 July	250	1.9*	45	1.76	~0	238	0.6	22	216
	6 Sept.–12 Oct.					–4.0	172	0.1	3	173
#24	15 Aug.–14 Sept.	5805	7.0	630	1.54	+4.5	177	0.6	10	162
#28	10–19 July	100	4.4*	0	1.61	~0	116	3.6	0	112

* Estimated.

Absorbed heat at a supraglacial pond surface, Q

Heat input to the water surface Q is expressed by the following equation involving shortwave radiation SR, longwave radiation LR, sensible heat flux H, latent heat flux E, heat flux with rainfall P, and heat flux with rockfall from the edge of the ice cliff F:

$$Q = SR + LR + H + E + P + F \quad (3)$$

All fluxes are taken to be positive when they are toward the water surface.

The net shortwave radiation was calculated by

$$SR = (1-\alpha)SR^{\downarrow} \tag{4}$$

Here $SR^{\downarrow}$ is the downward shortwave radiation and α is the albedo of the pond water, which depends on solar elevation h (in degrees). At Tsho Rolpa Glacier Lake in the Nepal Himalayas the following relationship was found during the monsoon season (Yamada, 1998):

$$\alpha = 0.78h^{-0.45} \tag{5}$$

The water was muddy, containing abundant suspended sediment. The turbidity was about 100 mg l^{-1}, and the transparency was less than 10 cm at the surface (Yamada, 1998). Turbidity of ponds on the Lirung Glacier was also high (50–300 mg l^{-1}). Therefore, almost all the shortwave radiation should be absorbed near the surface and would not reach the base of the pond.

Net radiation NR, downward shortwave radiation $SR^{\downarrow}$, upward shortwave radiation $SR^{\uparrow}$ and surface temperature T_{ms} were observed at the meteorological station, where the surface was debris covered. Downward longwave radiation $LR^{\downarrow}$ was estimated by:

$$LR^{\downarrow} = NR - SR^{\downarrow} + SR^{\uparrow} + \varepsilon_d \sigma T_{ms}^4 \tag{6}$$

Here ε_d is the emissivity of the debris surface (= 0.98) (Oke, 1978) and σ is the Stefan-Boltzmann constant. It was assumed that $LR^{\downarrow}$ was uniform over the ablation area, including the supraglacial ponds. Net longwave radiation incoming to the pond surface is hence expressed by:

$$LR = LR^{\downarrow} - \varepsilon_w \sigma T_s^4 \tag{7}$$

Here ε_w is the emissivity of the water surface (= 0.95) (Oke, 1978) and T_s is the surface water temperature (K).

Sensible and latent heat fluxes were calculated by bulk aerodynamic formulae presented by Kondo (1998), which were established for lake water surfaces with length from 1 to 10^4 m. Here, the bulk sensible and latent heat transfer coefficients are assumed to be equal, so that

$$H = c_p \rho_a CU(T_a - T_s) \tag{8}$$

$$E = l\rho_a CU(q_a - q_s) \tag{9}$$

where

$$C = 0.189\kappa\left[\ln\left(\frac{z}{z_0}\right)\right]^{-1}\left(\frac{X}{z_0}\right)^{-0.1} \tag{10}$$

Calculated values of C are summarized in Table 1. c_p, ρ_a and l are the specific heat of air at constant volume, air density at 4000 m a.s.l., and latent heat for evaporation from the water surface, respectively. U, q_a and q_s respectively represent the wind velocity at 1.5 m height, specific humidity of the air over the pond, and specific humidity at the pond surface q_s which is later assumed to be the saturated vapour pressure at the water

surface temperature T_s. κ, z, z_0, and X are Kalman constant, measurement height (1.5 m), roughness height (2.7×10^{-5} m), and the length of the pond surface, respectively.

When the temperature of rainfall is assumed to be equal to the air temperature the average heat flux from rainfall would be about 1.6 W m^{-2}. Usually rainfall is colder than the air, so the value of 1.6 W m^{-2} should be an upper limit. Since this heat flux is relatively small compared to other heat flux components, it was not included in the total heat input to the pond.

An upper limit for the heat flux from rockfall at the edge of the ice cliff surrounding pond #14 was estimated as follows. The pond area was 250 m^2 and was bordered by an ice cliff with a horizontal length of 20 m. The debris temperature was assumed to be a uniform 30°C, which was the maximum observed debris surface temperature. Average debris thickness measured at the ice cliff edges was about 1 m. The ice cliff retreat rate was 7.2 cm day^{-1} (Sakai *et al.*, 1998). The above data indicate the heat flux from a rockfall should be less than 3.5×10^{-4} W m^{-2}, which is negligible. There would also be a contribution of rock potential energy to the heat in the lake. A cliff height of 20 m predicts heating of the order of 1.0×10^{-2} W m^{-2}, which is also negligible.

Figure 5 shows an example of the absorbed heat balance components at pond #6. The net absorbed heat was dominated by shortwave radiation. The contributions for individual heat flux components are given in Table 1. The total heat input for the observed ponds ranged from 110 to 240 W m^{-2} with an average of 170 W m^{-2}. That heat would melt ice at a rate of 4.8 cm day^{-1} if it were dissipated over the same pond surface area.

Errors of the heat from shortwave radiation, longwave radiation, sensible and latent heat are ±3.5 W m^{-2}, ±23 W m^{-2}, 6.7 W m^{-2} and 5.1 W m^{-2}, respectively. The total error of the incoming heat to the pond surface is ±40 W m^{-2}.

Heat for icemelt, M_d, M_i and D

The ice at the bottom of the pond was covered with thick debris and sediment. The particle size was between clay and silt, and the permeability negligible (Terzaghi &

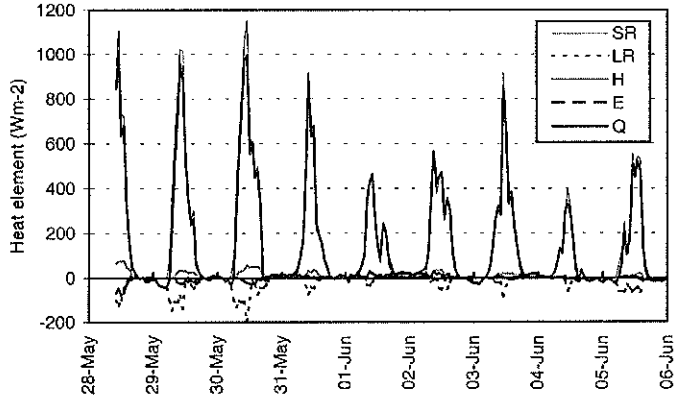

Fig. 5 Fluctuations in incoming heat elements (*SR*: shortwave radiation; *LR*: longwave radiation; *H*: sensible heat; *E*: latent heat; and *Q*: net absorbed heat) calculated at hourly intervals at pond #6 from 28 May to 5 June.

Peck, 1967). Therefore, convection in the debris is not possible and heat transfer is by conduction through the thickness of Δz. The thermal conductivity of the debris k was assumed to be 0.4 J K^{-1} m^{-1} s^{-1} like melting permafrost (Higashi, 1981). The heat flux M_d for unit area of the pond surface becomes

$$M_d = k\frac{T}{\Delta z}\cdot\frac{A_d}{A} \tag{11}$$

T is the temperature difference between water and the ice melting point, and A_d is the debris-covered area at the bottom of the pond, which was assumed to be equal to the pond surface area, A. The debris thickness at the bottom of the pond Δz was assumed to be the thickness observed at the edge of the ice cliff. On this basis, the heat available for melting under the debris layer at the bottom of the pond (M_d) was thus estimated to be approximately 1 W m^{-2} typically and 4 W m^{-2} maximum (Table 1). It is negligible in comparison with the heat incoming to the pond surface Q.

Weeks & Campbell (1973) applied an equation for the average heat transfer coefficient for the fully turbulent flow of a fluid over a flat plate (Eckert & Drake, 1959) to the melt rate of an iceberg at sea. Here, the expression was adopted for melt rate in pure water for application to the ponds as follows:

$$K = 7.14\times10^{-6}\left(\frac{v^{0.8}}{x^{0.2}}\right)\Delta T \tag{12}$$

where v and x are flow velocity of pond water (m s^{-1}) and the contact length of the ice with the water in the water flow direction (m). K is the melt rate (m s^{-1}). Equation (12) was adapted to icemelt in the pure water by changing the constant, which depends on the thermal conductivity, kinematic viscosity and specific heat of the fluid. The contact length x in equation (12) was assumed to be the vertical length of the bare ice in the pond. Since the temperature of the pond water was less than 4°C (temperature of maximum water density), heating from the surface would drive vertical circulation. The flow velocity of the pond was assumed to be less than 0.02 m s^{-1} since it was observed to be 0.02 m s^{-1} at the Tsho Rolpa Glacier Lake with ponds much larger than those on the Lirung Glacier. This prediction of heat transport to the submerged ice cliff gives the following melt rate per unit area of pond surface:

$$M_i = \rho_i L\cdot K\frac{A_i}{A} \tag{13}$$

where ρ_i, L and A_i are the respective density of ice, latent heat of icemelt and area of ice exposed under the water surface. In this calculation, the bare ice area in pond A_i was approximated from the horizontal length of the ice cliff and the average depth of the pond (Table 1). Observation of some ponds that drained suddenly showed that bare ice was restricted to the ice cliffs, so the above estimation of bare ice area should be reasonable. Calculated heat was at most 41 W m^{-2}, which was less than half of the absorbed heat at the pond surface Q.

The outflow heat D can be calculated as a residual value from equation (1) using the above estimates for Q, M_i, M_d and I, which indicates that D was at least 100 W m^{-2} (73% of Q) (Table 1).

Total melt amount for each type of surface

The surface of the debris-covered area can be divided into three kinds: ice cliffs, ponds and debris. The total heat absorbed by the whole debris-covered zone (8.9×10^{14} J or 28 W m^{-2}) is estimated from Rana *et al.* (1997). Our measurements provide estimates for the contribution from ice cliffs and ponds. The total for melt under the debris can then be estimated as a residual. Table 2 shows the total areas of each kind of surface and the corresponding total net heat absorbed over each area during the observation period. (The area of pond #1 was not included in the above total pond area, because its outflow heat was discharged directly out of the glacier (Fig. 1) and melt at the pond base during the observation period was negligible compared to the total heat absorbed by the ponds.) Although the absorbed heat per unit area was about 7 times greater on the ponds than the average for the whole debris-covered zone, the total absorbed in the ponds (0.25×10^{14} J) accounted for only 3% of the total absorbed over the debris-covered zone. The heat for icemelt under the surface debris (7.1×10^{14} J or 21 W m^{-2}) corresponds to an icemelt rate of 0.6 cm day^{-1}.

Table 2 Area and absorbed heat at each type of surface during the observation period (167 days) in 1996 on the Lirung Glacier.

	Whole debris-covered area	Pond	Ice cliff	Debris
Area (km^2)	2.30	0.01	0.04	2.16
Net absorbed heat (W m^{-2})	26*	170	256†	21
Net absorbed heat amount ($\times 10^{14}$ J)	8.9	0.3	1.5	7.1

* After Rana *et al.* (1997).
† After Sakai *et al.* (1998).

Water balance at the ponds

The heat discharged from the ponds D is substantial. In order to provide an additional check on the estimates of D, we estimate the water discharge q_o from a pond required to carry the heat out and examine whether melting in the watershed of the pond can provide that water. The required discharge is given by:

$$q_o = D/c_w \rho_w T_s \tag{14}$$

The corresponding water inflow is given from change in water storage and outflow as

$$q_i = A\frac{\mathrm{d}z_i}{\mathrm{d}t} + q_o \tag{15}$$

Figure 6 shows two examples (pond #6 and #24) of the inflow q_i calculated at 1-h intervals. The storage change was relatively small, possibly because the water level was controlled by spillways. Table 3 gives the mean daily inflows needed to transport D as calculated from equations (14) and (15) for ponds #6 and #24. Table 3 also shows the sources of water from ice cliffs (q_{ii}) and melting under the debris (q_{id}) that can provide the inflow. These sources were estimated as follows: q_{ii} was evaluated from the area of ice cliff surrounding each pond and the melt rate typical of ice cliffs

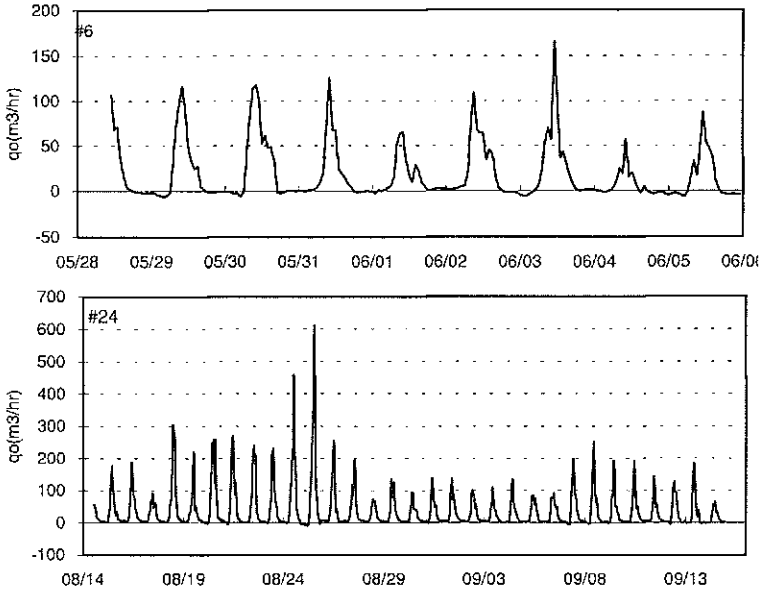

Fig. 6 Fluctuation of inflow to pond #6 and #24 at 1-h intervals calculated from equations (14) and (15).

(7.2 cm day^{-1}; Sakai *et al.*, 1998); q_{id} was calculated from the debris-covered area of the watershed indicated by the map from Aoki *et al.* (1998) and mean icemelt rate under the debris (0.6 cm day^{-1} from Table 2).

For pond #6 the required total inflow to transport D and the sum of the sources ($q_{ii} + q_{id}$) are essentially the same. This indicates an internal constancy that supports the heat balance calculations of the previous sections.

On the other hand, inferred inflow to transport D is much larger than estimated sources ($q_{ii} + q_{id}$) for pond #24. There are several possible explanations for this discrepancy. The discharge water temperature of pond #24 may have been higher than the surface water temperature observed locally. Given the relatively large size of pond #24, a sizeable temperature excess seems possible. A temperature about 6°C higher than observed would be required to account for the discrepancy. An additional source of water inflow from an englacial conduit could also help to explain it, but the englacial conduit would have to have a source area including more than half of the total debris-covered area or substantial input from the debris-free area. The latter supplies more than half of the total meltwater from glacier area (Rana *et al.*, 1997). Thus, this second explanation cannot be dismissed.

Table 3 Inflow amount estimated from heat discharge, D and inflow amount from ice cliff (q_{ii}) and from watershed debris-covered area (q_{id}) at ponds #6 and #24.

Pond no.	Inflow amount calculated from D (m^3 day^{-1})	q_{ii}: Area (m^2)	Meltwater amount (m^3 day^{-1})	q_{id}: Area (m^2)	Meltwater amount (m^3 day^{-1})	Total $q_{ii} + q_{id}$ (m^3 day^{-1})
#6	460	4 860	350	20 000	120	470
#24	13 810	11 400	820	123 000	738	1558

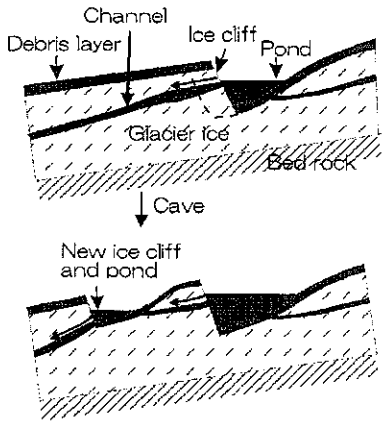

Fig. 7 Schematic figure of supraglacial pond formation by caving of the englacial water channel roof. The water channel enlarges as heat is absorbed at the pond surface, and the channel roof collapses to create a funnel-shaped depression. A new pond, surrounded by ice cliffs, is then formed. Formations of pond and ice cliffs accelerate the ablation rate at the debris-covered zone due to the high ablation rate at the pond and ice cliffs.

DISCUSSION

At least half of the heat absorbed at the surfaces of ponds was released with outflow. The melting caused by this heat is focused in the drainage paths such as englacial conduits or along the ice-debris interface of supraglacial trenches.

The temperature of water released from ponds should be close to the surface temperature (about 2°C). The potential for enlargement of englacial channels is considerable. (For example, Koizumi & Naruse (1994) found experimentally that 0.13°C water entering an initially small conduit of length 8 cm and initial diameter of 1.5 mm enlarged to 2.6 mm in a 13 minutes.) Some supraglacial ponds were observed suddenly to drain away during the melting season, probably by the thermal enlargement of their drainage channels or lowering of their floors. Although the absorbed heat at the ponds is smaller (0.3×10^{14} J) than the heat absorbed in the whole ablation zone (8.9×10^{14} J), its focused delivery to the ice could create large englacial or supraglacial channels.

Kirkbride (1993) suggested that supraglacial ponds aligned along an englacial conduit may be created by the collapse of the conduit roof. We suggest that heat absorbed in the ponds can accelerate this process by more rapid enlargement of the englacial conduit, roof collapse and formation of funnel-shaped hollows (Fig. 7). Even if water discharges from ponds along the debris–ice interface, the heat may melt trenches with overhanging bounding ice cliffs that can also collapse. Actually, funnel-shaped hollows appeared at three sites during the observation period, and they could be the sites of future ponds. Ice cliffs and the ponds absorb 10 and 7 times more heat than the debris-covered ice. Furthermore, absorbed heat at newly produced ponds could cause subsequent collapse of water channels and create more ice cliffs and ponds. This positive-feedback process could thereby accelerate the ablation rate of debris-covered glaciers.

Acknowledgements We wish to thank two anonymous reviewers and Charlie Raymond for their helpful comments and suggestions. We would like to express our

thanks to the Department of Hydrology and Meteorology, Ministry of Water Resources, His Majesty's Government of Nepal. We also thank Yutaka Ageta, Jumpei Kubota and all of the members of the Project for their valuable support getting these observations. Financial support was provided respectively, by a Grant-in-Aid for Scientific Research (Project no. 06041051, no. 09490018 and Aid for the Japan Society for the Promotion of Science (JSPS) Research Fellow) from the Ministry of Education, Science, Sports and Culture of the Japanese Government, and Cooperative Research under the Japan–US Cooperative Science Program from JSPS.

REFERENCES

Aoki, K. & Asahi, K. (1998) Topographical map of the ablation area of the Lirung Glacier in the Langtang Valley, Nepal Himalaya. *Bull. Glacier Res.* **16**, 19–31.

Eckert, E. R. G. & Drake, R. M. (1959) *Heat and Mass Transfer*. McGraw-Hill, New York.

Eyles, N. (1979) Facies of supraglacial sedimentation on Icelandic and Alpine temperate glaciers. *Can. J. Earth Sci.* **16**, 1341–1361.

Fujii, Y. (1977) Field experiment on glacier ablation under a layer of debris cover. *J. Japan. Soc. Snow Ice (Seppyo)* **39**, special issue, 20–21.

Fujii, Y. & Higuchi, K. (1977) Statistical analyses of the forms of the glaciers in Khumbu Himal. *J. Japan. Soc. Snow Ice (Seppyo)* **39**, special issue, 7–14.

Fujita, K., Sakai, A. & Chhetri, T. B. (1997) Meteorological observation in Langtang Valley, Nepal Himalayas, 1996. *Bull. Glacier Res.* **15**, 71–78.

Higashi, A. (1981) *Fundamentals of Cold Regions Engineering Science*. Kokon-shoin Co., Ltd Japan.

Inoue, J. & Yoshida, M. (1980) Ablation and heat exchange over the Khumbu Glacier. *J. Japan. Soc. Snow Ice (Seppyo)* **41**, special issue, 26–33.

Iwata, S., Watanabe, O. & Fushimi, H. (1980) Surface morphology in the ablation area of the Khumbu Glacier. *J. Japan. Soc. Snow Ice (Seppyo)* **41**, special issue, 9–17.

Kirkbride, M. P. (1993) The temporal significance of transitions from melting to calving termini at glaciers in the central Southern Alps of New Zealand. *The Holocene* 3(3), 232–240.

Koizumi, K & Narusc, R. (1994) Experiments on formation of water channels in a glacier (abstract in English). *J. Japan. Soc. Snow Ice (Seppyo)* **56**(2), 137–144.

Kondo, J. (ed.) (1998) *Meteorology in the Water Environment*. Asakura, Tokyo.

Mattson, L. E., Gardner, J. S. & Young, G. J. (1993) Ablation on debris covered glaciers: an example from the Rakhiot Glacier, Punjab, Himalaya. In: *Snow and Glacier Hydrology* (ed. by G. J. Young) (Proc. Kathmandu Symp., November 1992), 289–296. IAHS Publ. no. 218.

Nakawo, M., Moroboshi, T. & Uehara, S. (1993) Satellite data utilization for estimating ablation of debris covered glaciers. In: *Snow and Glacier Hydrology* (ed. by G. J. Young) (Proc. Kathmandu Symp., November 1992), 75–83. IAHS Publ. no. 218.

Oke, T. R. (1978) *Boundary Layer Climates*, second edn. John Wiley, New York.

Østrem, G. (1959) Ice melting under a thin layer of moraine and the existence of ice cores in moraine ridges. *Geogr. Ann.* **41**, 228–230.

Rana, B., Nakawo, M., Fukushima, Y. & Ageta, Y. (1997) Application of a conceptual precipitation–runoff model (HYCYMODEL) in a debris-covered glacierized basin in the Langtang Valley, Nepal Himalaya. *Ann. Glaciol.* **25**, 226–231.

Sakai, A., Nakawo, M. & Fujita, K. (1998) Melt rate of ice cliffs on the Lirung Glacier, Nepal Himalayas, 1996. *Bull. Glacier Res.* **16**, 57–66.

Terzaghi, K. & Peck, R. B. (1967) *Soil Mechanics in Engineering Practice*, second edn. John Wiley & Sons, Inc., New York.

Weeks, W. F. & Campbell, W. J. (1973) Iceberg as a fresh-water source: an appraisal. *J. Glaciol.* **12**, 65, 207–233.

Yamada, T. (1998) *Glacier Lake and its Outburst Flood in the Nepal Himalaya*. Monograph no. 1, March 1998, Data Centre for Glacier Research, Japanese Society of Snow and Ice.